Atmos. Chem. Phys., 15, 13133–13144, 2015
www.atmos-chem-phys.net/15/13133/2015/
doi:10.5194/acp-15-13133-2015


Atmospheric Chemistry and Physics Open Access EGU

# Estimating ground-level $PM_{2.5}$ in eastern China using aerosol optical depth determined from the GOCI satellite instrument

**J.-W. Xu[1], R. V. Martin[1,2], A. van Donkelaar[1], J. Kim[3], M. Choi[3], Q. Zhang[4,5], G. Geng[4,5], Y. Liu[6], Z. Ma[6,7], L. Huang[7], Y. Wang[4,8,9], H. Chen[10], H. Che[11], P. Lin[12], and N. Lin[13]**

[1]Department of Physics and Atmospheric Science, Dalhousie University, Halifax, Canada
[2]Harvard-Smithsonian Center for Astrophysics, Cambridge, Massachusetts, USA
[3]Department of Physics and Atmospheric Sciences, Yonsei University, Seoul, South Korea
[4]Ministry of Education Key Laboratory for Earth System Modeling, Center for Earth System Science, Institute for Global Change Studies, Tsinghua University, Beijing, China
[5]State Key Joint Laboratory of Environment Simulation and Pollution Control, School of Environment, Tsinghua University, Beijing, China
[6]Department of Environmental Health, Rollins School of Public Health, Emory University, Atlanta, GA, USA
[7]State Key Laboratory of Pollution Control and Resource Reuse, School of the Environment, Nanjing University, Nanjing, China
[8]Department of Marine Sciences, Texas A&M University at Galveston, Galveston, Texas, USA
[9]Department of Atmospheric Sciences, Texas A&M University, College Station, Texas, USA
[10]Institute of Atmospheric Physics, Chinese Academy of Sciences, Beijing, China
[11]Institute of Atmospheric Composition, Chinese Academy of Meteorological Sciences, Beijing, China
[12]Department of Atmospheric Sciences, National Taiwan University, Taipei, Taiwan
[13]Department of Atmospheric Sciences, National Central University, Taoyan, Taiwan

*Correspondence to:* J.-W. Xu (junwei.xu@.dal.ca)

Received: 1 May 2015 – Published in Atmos. Chem. Phys. Discuss.: 24 June 2015
Revised: 13 November 2015 – Accepted: 13 November 2015 – Published: 27 November 2015

**Abstract.** We determine and interpret fine particulate matter ($PM_{2.5}$) concentrations in eastern China for January to December 2013 at a horizontal resolution of 6 km from aerosol optical depth (AOD) retrieved from the Korean geostationary ocean color imager (GOCI) satellite instrument. We implement a set of filters to minimize cloud contamination in GOCI AOD. Evaluation of filtered GOCI AOD with AOD from the Aerosol Robotic Network (AERONET) indicates significant agreement with mean fractional bias (MFB) in Beijing of 6.7 % and northern Taiwan of −1.2 %. We use a global chemical transport model (GEOS-Chem) to relate the total column AOD to the near-surface $PM_{2.5}$. The simulated $PM_{2.5}$ / AOD ratio exhibits high consistency with ground-based measurements in Taiwan (MFB = −0.52 %) and Beijing (MFB = −8.0 %). We evaluate the satellite-derived $PM_{2.5}$ versus the ground-level $PM_{2.5}$ in 2013 measured by the China Environmental Monitoring Center. Significant agreement is found between GOCI-derived $PM_{2.5}$ and in situ observations in both annual averages ($r^2 = 0.66$, $N = 494$) and monthly averages (relative RMSE = 18.3 %), indicating GOCI provides valuable data for air quality studies in Northeast Asia. The GEOS-Chem simulated chemical composition of GOCI-derived $PM_{2.5}$ reveals that secondary inorganics ($SO_4^{2-}$, $NO_3^-$, $NH_4^+$) and organic matter are the most significant components. Biofuel emissions in northern China for heating increase the concentration of organic matter in winter. The population-weighted GOCI-derived $PM_{2.5}$ over eastern China for 2013 is 53.8 μg m$^{-3}$, with 400 million residents in regions that exceed the Interim Target-1 of the World Health Organization.

**Published by Copernicus Publications on behalf of the European Geosciences Union.**

## 1 Introduction

Fine particulate matter with aerodynamic diameter less than 2.5 μm ($PM_{2.5}$) is a robust indicator of mortality and other negative health effects associated with ambient air pollution (Goldberg, 2008; Laden et al., 2006). It is estimated that more than 3 million people lost their lives prematurely due to $PM_{2.5}$ in 2010 (Lim et al., 2012), of which 1 million occurred in East Asia (Silva et al., 2013). In China, there have already been several episodes with $PM_{2.5}$ described as "beyond index" levels. Thus, it is of paramount importance to monitor $PM_{2.5}$ concentration across China. Satellite remote sensing has a high potential to monitor $PM_{2.5}$.

Satellite retrievals of aerosol optical depth (AOD), which provide a measure of the amount of light extinction through the atmospheric column due to the presence of aerosols, have long been recognized to relate to ground level $PM_{2.5}$ (Wang and Christopher, 2003). Many studies have developed advanced statistical relationships to estimate with high accuracy surface $PM_{2.5}$ from satellite AOD (Liu et al., 2009; Kloog et al., 2012; Hu et al., 2013). For example, Ma et al. (2014) estimated $PM_{2.5}$ concentrations in China from satellite AOD by developing a national-scale geographically weighted regression model, and found strong agreement ($r^2 = 0.64$) with ground measurements.

In addition to empirical statistical methods, satellite AOD can also be geophysically related to surface $PM_{2.5}$ by the use of a chemical transport model to simulate the $PM_{2.5}$ to AOD relationship (Liu et al., 2004; van Donkelaar et al., 2010). This approach was first demonstrated using data from the Multiangle Imaging Spectroradiometer (MISR) aboard NASA's Terra satellite over the United States for 2001 (Liu et al., 2004). Van Donkelaar et al. (2006, 2010) extended this approach to estimate $PM_{2.5}$ from AOD retrieved from both the MODIS (Moderate Resolution Imaging Spectroradiometer) and the MISR satellite instruments, and developed a long-term global estimate of $PM_{2.5}$ at a spatial resolution of approximately 10 km × 10 km. Boys et al. (2014) used AOD retrieved from MISR and the SeaWiFS (Sea-Viewing Wide Field-of-View Sensor) to produce a 15-year (1998–2012) global trend of ground-level $PM_{2.5}$. These previous studies have proven to be globally effective, but more detailed regional investigation is needed in densely polluted and populated regions like China.

The Geostationary Ocean Color Imager (GOCI) is the first geostationary satellite instrument that offers multi-spectral aerosol optical properties in Northeast Asia (Park et al., 2014). GOCI has a high observation density of eight retrievals per day (hourly retrievals from 09:00 to 16:00 Korean Standard Time) over a location, which exceeds the retrieval density of traditional low-Earth polar-orbiting satellite instruments. Thus, GOCI is promising for more detailed investigations on aerosol properties in highly polluted and populated regions including eastern China.

In this study, we estimate ground-level $PM_{2.5}$ in eastern China for 2013 at a horizontal resolution of 6 km by 6 km, by using AOD retrieved from GOCI, coupled with the relationship of $PM_{2.5}$ to AOD simulated by a chemical transport model (GEOS-Chem). Section 2 describes the approach and data. Section 3 evaluates the GOCI AOD, the simulated $PM_{2.5}$ to AOD relationship, and the GOCI-derived $PM_{2.5}$ using recently available ground-level measurements from the China Environmental Monitoring Center (http://113.108.142:20035/emcpublish/). We also interpret the GOCI-derived $PM_{2.5}$ by using the GEOS-Chem model to estimate its chemical composition. Section 4 summarizes the major findings and potential future improvements of the current analysis.

## 2 Methods

### 2.1 Aerosol optical depth from the GOCI satellite instrument

GOCI operates onboard the Communication, Ocean, and Meteorology Satellite (COMS) that was launched in 2010 in Korea (Lee et al., 2010). The spatial coverage of GOCI is 2500 km × 2500 km in Northeast Asia, including eastern China, the Korean peninsula and Japan (Kang et al., 2006). GOCI has eight spectral channels for aerosol retrievals, including six visible bands at 412, 443, 490, 555, 660, 680 nm and two near infrared bands at 745 and 865 nm (Park et al., 2014). The Level 2 AOD products are retrieved at a spatial resolution of 6 km by 6 km, using a clear-sky composite method for surface reflectance and a lookup table approach based on AERONET observations (Lee et al., 2010, 2012).

A challenge using GOCI to detect aerosols in the atmosphere is the absence of mid-infrared (IR) channels to detect clouds, which means that significant errors could be induced in the estimates of AOD. The operational GOCI products screen clouds based on spatial variability and threshold tests at each 6 km × 6 km pixel in combination with a meteorological imager that has four IR channels (at 3.7, 6.7, 10.8, 12 μm wavelengths) at 4 km by 4 km resolution onboard the same satellite (Cho and Youn, 2006). However, as will be shown here, cloud contamination still occurs. Therefore, we apply a set of spatial filters following Hyer et al. (2011) and temporal filters to further eliminate cloud contamination in GOCI AOD. The filters include (1) a buddy check that sets a minimum number of 15 retrievals per 30 km × 30 km grid cell, (2) a local variance check to eliminate grid cells where the coefficient of variation of AOD is larger than 0.5 within the surrounding 5 × 5 grid cells and (3) a diurnal variation check that excludes grid cells with diurnal variation (maximum – minimum) of AOD larger than 0.74 which is the 90th percentile of diurnal variation of AERONET AOD in Beijing and northern Taiwan for 2013. In this study, we use

GOCI AOD for January–December 2013 to derive ground-level $PM_{2.5}$ in eastern China.

### 2.2 Aerosol optical depth from AERONET ground-based measurements

The Aerosol Robotic Network (AERONET) is a globally distributed network of CIMEL Sun photometers (Holben et al., 1998) that provide multi-wavelength AOD measurements with a low uncertainty of < 0.02 (Holben et al., 2001). Here we use AERONET Level 1.5 cloud screened data (Smirnov et al., 2000) for January–December 2013 from four stations within the GOCI domain: Beijing, Beijing-CAMS, Taipei_CWB and EPA-NCU. AERONET Level 2 data for 2013 are not available for some stations discussed in this paper. Thus, we use Level 1.5 for consistency. We compared Level 2 and Level 1.5 data for 2013 for stations that do have Level 2 available, and found Level 1.5 AOD is highly consistent with Level 2 AOD with RMSE of 0.01–0.02 (relative RMSE of 2–7 %). Criteria for selecting an AERONET station are (1) a $PM_{2.5}$ ground monitor has to be located within 10 km and (2) a complete time series of AOD data records for the period of study has to be available. Beijing and Beijing-CAMS stations are located in downtown Beijing, with the closest available $PM_{2.5}$ monitors 9.5 and 7.5 km away, respectively. However, due to interrupted time series of $PM_{2.5}$ records at both these stations, we combine the AERONET AOD from the Beijing and Beijing-CAMS stations and $PM_{2.5}$ from the corresponding two in situ ground-based sites as a "combined Beijing" site. Taipei_CWB and EPA-NCU stations are located in populated northern Taiwan, with nearly collocated $PM_{2.5}$ monitors (< 3 km). We similarly combine the Taipei_CWB and EPA-NCU as "northern Taiwan" site. We use these sites to evaluate GOCI AOD and the relationship between AOD and $PM_{2.5}$ simulated by a global chemical transport model.

### 2.3 Simulation of the relationship between AOD and $PM_{2.5}$ by GEOS-Chem

We use the GEOS-Chem chemical transport model (version 9-01-03; http://geos-chem.org) to calculate the spatiotemporally resolved relationship between ground-level $PM_{2.5}$ and satellite-retrieved column AOD.

Our nested GEOS-Chem simulation at $1/2^\circ \times 2/3^\circ$ spatial resolution with 47 vertical levels (14 levels in the lowest 2 km) is driven by assimilated meteorology from the Goddard Earth Observing System (GEOS-5). A global simulation at $2^\circ \times 2.5^\circ$ spatial resolution is used to provide boundary conditions for the nested domain (Wang et al., 2004). We spin up the model for 1 month before each simulation to remove the effects of initial conditions on the aerosol simulation.

GEOS-Chem includes a fully coupled treatment of tropospheric oxidant–aerosol chemistry (Bey et al., 2001; Park et al., 2004). The GEOS-Chem aerosol simulation includes the sulfate-nitrate-ammonium system (Park et al., 2004; Pye et al., 2009), primary (Park et al., 2003) and secondary (Henze and Seinfeld, 2006; Henze et al., 2008; Liao et al., 2007; Fu et al., 2008) organics, mineral dust (Fairlie et al., 2007), and sea salt (Jaeglé et al., 2011). We estimate the concentration of organic matter (OM, which includes elements such as hydrogen, oxygen and nitrogen) from the simulated primary organic carbon (OC) using spatially and seasonally resolved values from OMI (Ozone Monitoring Instrument) $NO_2$ and AMS (aerosol mass spectrometer) measurements following Philip et al. (2014). Gas-aerosol phase partitioning is simulated using the ISORROPIA II thermodynamic scheme (Fountoukis and Nenes, 2007). GEOS-Chem calculates AOD using relative humidity-dependent aerosol optical properties following Martin et al. (2003). Dust optics are from Ridley et al. (2012).

Anthropogenic emissions are based on the Multi-resolution Emission Inventory for China (MEIC; http://www.meicmodel.org) for 2010, and the Zhang et al. (2009) inventory for surrounding East Asia regions for 2006. Both inventories are scaled to the simulation year (2012–2013), following Ohara et al. (2007). Non-anthropogenic emissions include biomass burning emissions (GFED-3) (Mu et al., 2011), biogenic emissions (MEGAN) (Guenther et al., 2006), soil $NO_x$ (Yienger and Levy, 1995; Wang et al., 1998), lightning $NO_x$ (Murray et al., 2012), aircraft $NO_x$ (Wang et al., 1998; Stettler et al., 2011), ship $SO_2$ from EDGAR (Olivier and Berdowski, 2001) and volcanic $SO_2$ emissions (Fischer et al., 2011). $HNO_3$ concentrations are artificially decreased to 75 % of their values at each timestep following Heald et al. (2012) to account for regional bias (Wang et al., 2013). Emissions are distributed into the lower mixed layer, with a correction to the GEOS-5 predicted nighttime mixing depths following Heald et al. (2012) and Walker et al. (2012).

We apply GEOS-Chem to simulate daily relationships between ground level $PM_{2.5}$ and column AOD, specifically $PM_{2.5}$ / AOD. $PM_{2.5}$ concentrations are calculated at 35 % relative humidity for consistency with in situ measurements. For consistency with GOCI AOD and $PM_{2.5}$ ground-based measurements, we sample the simulated AOD only from hours that GOCI has retrievals (00:00–07:00 UTC), and calculate the simulated daily $PM_{2.5}$ from 24 h averages as reported for the ground-based $PM_{2.5}$ measurements. The simulation period is May 2012–April 2013 as the GEOS-5 meteorological fields are not available afterward. The mismatch with observations for May–December 2013 has the potential to degrade performance, but as will be shown here no clear loss of quality is apparent.

### 2.4 In situ $PM_{2.5}$ measurements

We collect $PM_{2.5}$ measurements from 494 monitors to evaluate the GOCI-derived values. In situ $PM_{2.5}$ daily measurements in Mainland China for 2013 are primarily from

the official website of the China Environmental Monitoring Center (CEMC; http://113.108.142:20035/emcpublish/). Data are also collected from some provinces (e.g., Shandong, Zhejiang) and municipalities (e.g., Beijing and Tianjin) with additional sites that are not included in the CEMC website. Daily in situ $PM_{2.5}$ data in northern Taiwan for 2013 are from the Taiwan Environmental Protection Administration (TEPA; http://taqm.epa.gov.tw). The in situ $PM_{2.5}$ data in both Mainland China and northern Taiwan are measured by a collection of the tapered element oscillating microbalance methods (TEOMs) and beta-attenuation methods (BAMs) with some TEOMs being heated to 30 °C and others to 50 °C (CNAAQS, GB3095-2012, 2012; http://taqm.epa.gov.tw). The specific instrument (BAMs or TEOMs) used by each monitoring site is unknown. The effective relative humidity of the resultant $PM_{2.5}$ measurement likely varies diurnally and seasonally as a function of the ambient temperature. Semivolatile losses are expected from the TEOMs. The network design appears to include compliance objectives that may affect monitor placement. Despite these issues, we use the monitoring data to evaluate our satellite-derived $PM_{2.5}$ since the monitoring data offer valuable information about ground-level $PM_{2.5}$ concentrations. We also collect $PM_{2.5}$ measurements from a monitor in Beijing as part of the surface particulate matter Network (SPARTAN; www.spartan-network.org) using a three-wavelength nephelometer and an impaction filter sampler (Snider et al., 2015). The SPARTAN, CEMC and TEPA $PM_{2.5}$ monitoring data combined with AERONET AOD are used to estimate the empirical relationship between $PM_{2.5}$ and AOD, and to further evaluate the relationship simulated by the model.

### 2.5 Statistical terms

Root mean square error (RMSE), relative root mean square error (rRMSE), mean fractional bias (MFB) and mean fractional error (MFE) are defined as

$$\mathrm{RMSE} = \sqrt{\frac{1}{N}\sum_{i=1}^{N}(S_i - O_i)^2} \quad (1)$$

$$\mathrm{rRMSE} = \frac{\mathrm{RMSE}}{\frac{1}{N}\sum_{i=1}^{N} O_i} \quad (2)$$

$$\mathrm{MFB} = \frac{1}{N}\sum_{i=1}^{N}\frac{(S_i - O_i)}{\left(\frac{S_i+O_i}{2}\right)} \times 100\,\% \quad (3)$$

$$\mathrm{MFE} = \frac{1}{N}\sum_{i=1}^{N}\frac{|S_i - O_i|}{\left(\frac{S_i+O_i}{2}\right)} \times 100\,\%, \quad (4)$$

where $S_i$ is the satellite-derived value of the parameter in question, $O_i$ is the corresponding observed value, and $N$ is the number of observations.

Coefficient of variation (CV) is defined as

$$\mathrm{CV} = \frac{\text{Standard deviation}}{\text{Mean}} \quad (5)$$

## 3 Results and discussion

### 3.1 Evaluation of satellite AOD and the simulated relationship between $PM_{2.5}$ and AOD

Figure 1 shows the effects of our cloud-screening filters on GOCI AOD. The left panel shows GOCI true color images from 5 July 2013 at 10:30 (top) and 11:30 (bottom) Korean Standard Time. The boxes identify challenging regions with thick white cloud, dark cloud-free oceans and gray shading that appears to be thin cloud. The operational GOCI AOD retrievals, shown in the middle panel, correctly exclude thick clouds, but report high AOD for the potentially thin clouds. Although these gray regions could contain aerosol, we err on the side of caution. Application of our additional temporal and spatial cloud filters removes the suspicious pixels from the original GOCI data, as shown in the right panel. Our filters reject 10.3 % of all the operational GOCI AOD data investigated in this study. We evaluate the cloud filters further below.

Figure 2 (top) shows monthly averages of coincident filtered hourly GOCI and AERONET AOD for January–December 2013 at combined Beijing and northern Taiwan stations. GOCI AOD is highly consistent with AERONET observations with MFB of 6.7 % in Beijing and −1.2 % in Taiwan. GOCI AOD and AERONET AOD are positively skewed at both stations, and the skewness is reduced in GOCI AOD at both stations due to more records for extremely small AOD (< 0.04) in GOCI products. The relatively larger rRMSE between GOCI and AERONET AOD in northern Taiwan may reflect the fewer observations there.

We investigate the filtered diurnal variation of GOCI AOD at the above AERONET stations and find the level of AOD is uniform within a day (e.g., the coefficient of variation in Beijing is 0.1), similar to AERONET observations.

The effect of excluding our cloud-screening filters is negligible for coincident comparisons with AERONET since AERONET is already cloud-screened. The exclusion of our cloud filters for a non-coincident comparison that includes all GOCI data would introduce significant error versus AERONET observations, increasing rRMSE by a factor of 1.7–3.3 in Beijing and northern Taiwan. Changing the buddy check threshold in our cloud filters from 15 to 10 would significantly underestimate AOD especially in northern Taiwan where the MFB would increase from −1.2 to −15.0 %. Decreasing the threshold of local variance check to 0.4 has little influence (< 0.1 %) for rRMSE, MFB and MFE, but would have larger influence on GOCI-derived $PM_{2.5}$ as will be shown later. Limiting the diurnal variation of GOCI AOD to the 80th percentile of diurnal variations in observations would introduce bias (rRMSE would increase by 4 % in Beijing) to GOCI AOD. As will be shown here, GOCI-derived $PM_{2.5}$ offers an additional test of cloud screening filters. Figure 2 (bottom) shows the relationship between the ground level $PM_{2.5}$ and the columnar AOD as simulated by GEOS-

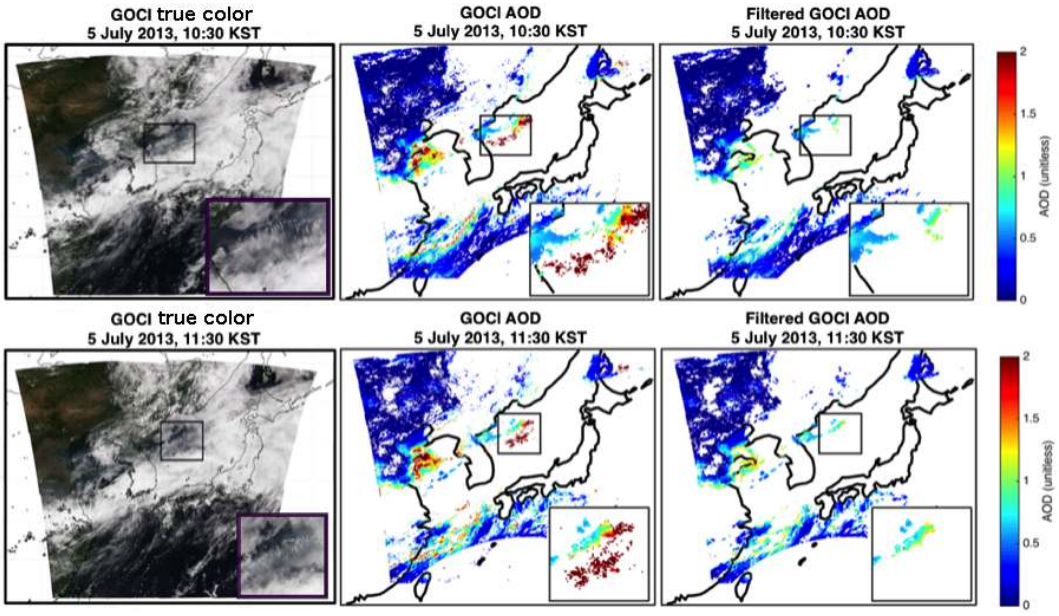


**Figure 1.** The GOCI granules from 5 July 2013, 10:30 (top) and 11:30 (bottom) Korean Standard Time. From left to right on each panel are the GOCI true color images, the operational AOD retrievals and the AOD retrievals after applying temporal and textual filters to reduce cloud contamination. The boxes highlight examples of challenging cloud fields, and are enlarged within the lower right subplot of each panel.

Chem and from ground-based measurements. The measured ratio in Beijing has pronounced seasonal variation with values high in winter and low in spring. The measured ratio in northern Taiwan exhibits little seasonal variation. The annual mean GEOS-Chem $PM_{2.5}$ / AOD ratio well reproduces the ground-based measurements despite the temporal inconsistency of the two metrics for May–December. The simulation captures the pronounced seasonal variation in Beijing and the comparably aseasonal behavior in northern Taiwan. The simulated seasonal variation of $PM_{2.5}$ / AOD in Beijing arises from the seasonal variation of mixed-layer depth (factor of 2 higher in summer than winter) combined with the near-constant columnar AOD throughout the year as shown in Fig. 2 (top).

Snider et al. (2015) interpreted coincident measurements of AOD, $PM_{2.5}$, and nephelometer measurements of aerosol scattering and found that the temporal variation of the $PM_{2.5}$ / AOD ratio in Beijing was primarily driven by the vertical profile in aerosol scattering. We examine the seasonal variation in the simulated $PM_{2.5}$ / AOD and similarly find that the ratio of ground-level aerosol scatter to columnar AOD contributes most (89 %) of the monthly variability in the $PM_{2.5}$ / AOD ratio in Beijing.

### 3.2 Evaluation of ground-level $PM_{2.5}$ derived from GOCI AOD

Figure 3 shows the seasonal and annual distribution of $PM_{2.5}$ over East Asia at a spatial resolution of 6 km by 6 km for 2013. In both GOCI-derived and measured $PM_{2.5}$, winter concentrations in eastern China exceed 100 $\mu g\,m^{-3}$ over vast regions, with lower values in summer. Both GOCI-derived and in situ measurements reveal that $PM_{2.5}$ in northern China is higher than in southern China, especially for the Beijing, Hebei and Shandong provinces where the annual $PM_{2.5}$ is almost 100 $\mu g\,m^{-3}$ or more. Prior work has attributed this regional enhancement to high emission rates (Zhao et al., 2013; Zhang et al., 2013) that in part arises from emissions when producing goods for exports (Jiang et al., 2015).

Figure 4 compares annual and seasonal averages of daily ground-measured $PM_{2.5}$ from 494 sites with coincident daily GOCI-derived $PM_{2.5}$ from pixels that contain the ground-based sites. A significant correlation ($r^2 = 0.66$, $N = 494$) with a slope near unity (1.01) is found in the annual scatter plot. The slope remains near unity (0.95–1.01) in seasonal scatter plots. The weaker correlation for all four seasons implies random representativeness differences between point in situ measurements and area-averaged satellite values when data density diminishes. Semivolatile losses from some in situ instruments (TEOMs) might contribute to scatter in winter when nitrate constitutes a larger fraction of $PM_{2.5}$. We focus on more meaningful aggregated measurements. Using the same technique, we also estimated $PM_{2.5}$ from MODIS Collection 6 AOD for 2013, and found GOCI-derived $PM_{2.5}$ achieves greater consistency than MODIS-derived $PM_{2.5}$ when compared with ground-based measurements (slope = 1.1, $r^2 = 0.61$). GOCI-derived $PM_{2.5}$ also corrects the significant underestimation of $PM_{2.5}$ from GEOS-Chem (slope = 0.68, $r^2 = 0.85$) when compared with ground measurements.

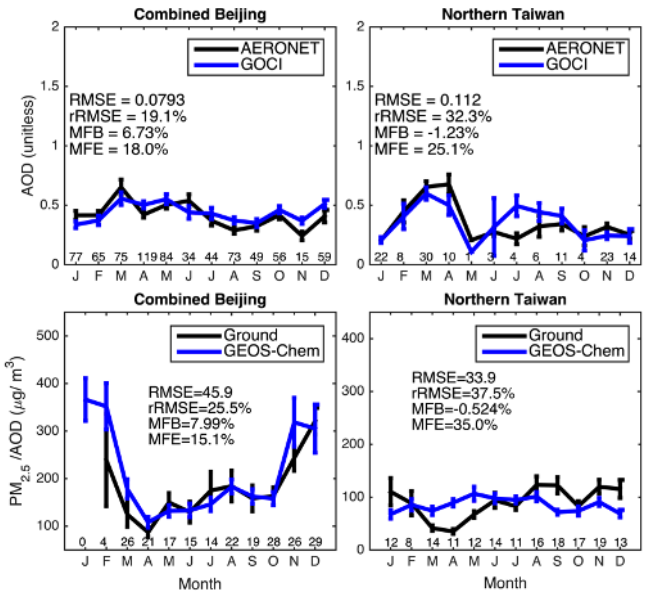


**Figure 2.** Top: monthly time series of AOD from AERONET and GOCI for January–December 2013. Numbers above the $x$ axis denote the number of coincident hourly observations in each month. Bottom: monthly averages of $PM_{2.5}$ / AOD from ground measurements and the GEOS-Chem simulation at AERONET sites. The ground-based ratio is sampled from daily ground $PM_{2.5}$ coincident with AERONET AOD for January–December 2013. The GEOS-Chem simulation is for May 2012–April 2013, noncoincident with the ground-based ratio for May–December 2013. Numbers above the $x$ axis denote the number of daily ground-based observations in each month. Error bars represent standard errors. Statistics are root mean square error (RMSE), relative root mean square error (rRMSE), mean fractional bias (MFB) and mean fractional error (MFE).

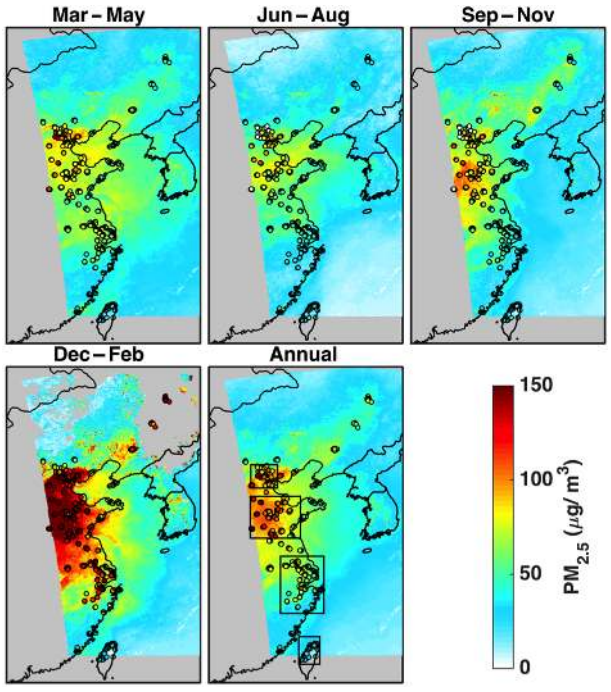


**Figure 3.** Seasonal and annual distribution of $PM_{2.5}$ concentrations at 6 km by 6 km resolution over East Asia for 2013. The background color indicates averages of GOCI-derived daily surface $PM_{2.5}$ concentrations. Filled circles represent averages of daily ground-based measurements of $PM_{2.5}$. Gray denotes missing values. Boxes in the annual map denote regions used for monthly comparisons in Fig. 5 from top to bottom: Beijing and surrounding areas, Shandong and surrounding regions, Shanghai and surrounding areas and northern Taiwan.

Figure 5 shows monthly averages of GOCI-derived $PM_{2.5}$ and in situ measurements at four regions outlined in Fig. 3. Regions are selected based on the level of $PM_{2.5}$ concentration and the population of residents. A high degree of consistency is found in all regions. Both data sets show more seasonal variation in northern regions like Beijing and Shandong than southern regions like Shanghai and northern Taiwan. Both indicate that $PM_{2.5}$ concentrations in northern regions are generally higher than in southern regions. The exclusion of our cloud screening filters from the GOCI AOD would introduce significant bias in GOCI-derived $PM_{2.5}$ versus ground-based measurements especially in summer, increasing rRMSE by a factor of 1.7–5.3 in all four regions. Changing the threshold of local variance check in our cloud filters to 0.4 would introduce bias by restricting the variation of $PM_{2.5}$ concentrations. For example, GOCI-derived $PM_{2.5}$ would be generally underestimated in Beijing areas (rRMSE = 16.6 % and MFB = −6.8 %) and Shandong areas (rRMSE = 16.6 % and MFB = −3.42 %).

### 3.3 Seasonal variation of $PM_{2.5}$

Figure 6 shows the monthly averages of coincident daily GOCI-derived and in situ $PM_{2.5}$ concentrations for the domain of eastern China. Both the GOCI-derived $PM_{2.5}$ and ground-based observations exhibit similar seasonal variation with values high in winter and low in summer. Exclusion of our temporal and spatial cloud-screening filters from GOCI-derived $PM_{2.5}$ would increase rRMSE by a factor of 3.4. Figure 6 also shows the chemical composition of GOCI-derived $PM_{2.5}$, as calculated by applying the GEOS-Chem simulated mass fraction of $PM_{2.5}$ chemical components to GOCI-derived $PM_{2.5}$ mass concentration. Aerosol water is attached to each component according to its hygroscopicity. Secondary inorganic aerosols (SIA; $SO_4^{2-}$, $NO_3^-$, $NH_4^+$) are the most abundant components throughout the year, accounting for 65 % of $PM_{2.5}$ concentrations, followed by OM (18 %). The $NO_3^-$ and OM concentrations increase by a factor of 2 in winter, together comprising most of $PM_{2.5}$ (31 % for $NO_3^-$ and 26 % for OM). Summer is predominately controlled by SIA (74 %). Dust plays an important role in spring (15 %) and fall (15 %). Our seasonal variation of chemical

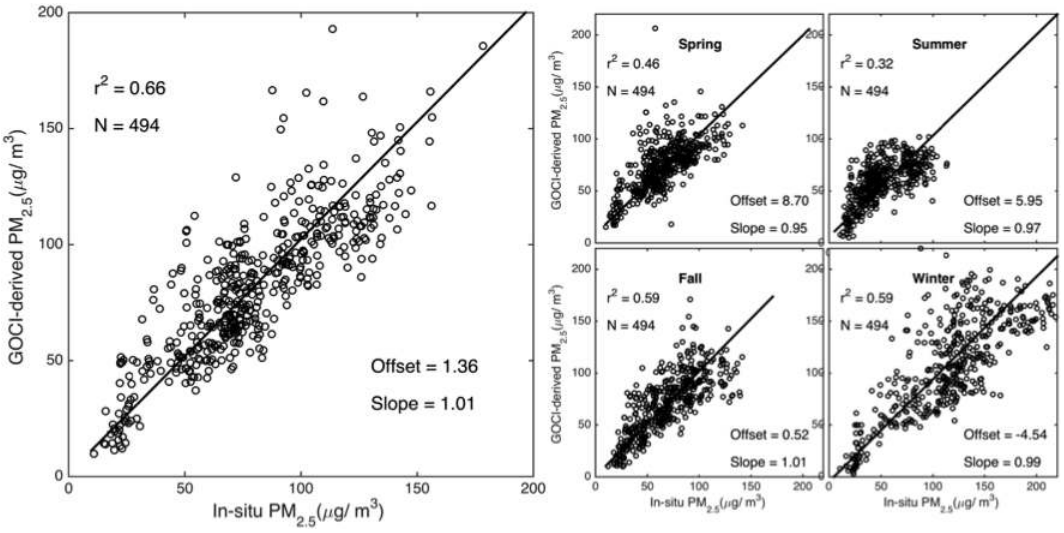


**Figure 4.** Scatterplots of the annual mean (left) and seasonal mean (right) GOCI-derived $PM_{2.5}$ for 2013 against $PM_{2.5}$ from 494 ground monitors over the GOCI domain in eastern China.

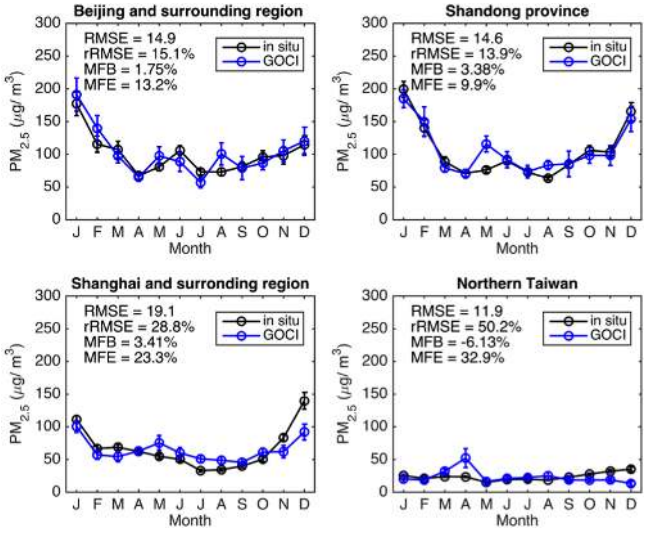


**Figure 5.** Monthly averages of daily $PM_{2.5}$ from in situ measurements and daily $PM_{2.5}$ estimated from GOCI AOD for 2013. Regions are defined in Fig. 3. Error bars represent standard errors. Statistics are root mean square error (RMSE), relative root mean square error (rRMSE), mean fractional bias (MFB) and mean fractional error (MFE).

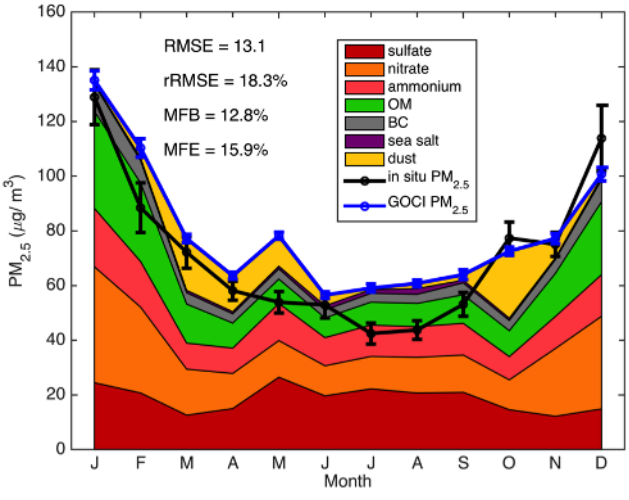


**Figure 6.** Monthly variation of GOCI-derived $PM_{2.5}$ and in situ $PM_{2.5}$ for 2013 over eastern China, with chemical composition for GOCI-derived $PM_{2.5}$. The in situ $PM_{2.5}$ is determined from the averages of all ground stations in eastern China for 2013 and GOCI-derived $PM_{2.5}$ is calculated from the average of all grid boxes that contain $PM_{2.5}$ ground monitors. The chemical composition is calculated by applying the GEOS-Chem simulated mass fraction of $PM_{2.5}$ chemical components to GOCI-derived $PM_{2.5}$ mass concentration. Aerosol water is associated with each $PM_{2.5}$ component according to its hygroscopicity. Error bars represent standard errors.

composition is generally consistent with ground-based measurements in previous works across eastern China. A number of studies in Beijing, the Yangtze River delta and Pearl River delta regions all reported that OM and SIA are the most important components of $PM_{2.5}$ through the year (He et al., 2001; Ye et al., 2003; Tao et al., 2012; Zhang et al., 2013). Zhang et al. (2008) showed consistent seasonal patterns in OM at 18 stations in China, with a winter maximum, and a summer minimum, similar to the seasonality of OM in this work. Zhang et al. (2013) studied the chemical composition of $PM_{2.5}$ in Beijing and found the percentage of SIA in $PM_{2.5}$ is largest in summer, consistent with our result.

The seasonal variation of $PM_{2.5}$ in Fig. 6 is driven by a combination of meteorological conditions, emissions, and nitrate formation. All three processes have greater seasonal

**Table 1.** Annual $PM_{2.5}$ concentrations, area-weighted concentrations of chemical composition and affected population of $PM_{2.5}$ in regions outlined in Fig. 3 and in overall eastern China (excluding northern Taiwan) for 2013. Aerosol water is not associated with each $PM_{2.5}$ component for consistency with measurement protocols. $PM_{2.5}$ concentration is at 35 % relative humidity. IT1 refers to the WHO air quality interim target-1 of $35\,\mu g\,m^{-3}$.

| Region | Beijing | Shandong | Shanghai | Eastern China | Northern Taiwan |
|---|---|---|---|---|---|
| Population-weighted GOCI-derived $PM_{2.5}$ ($\mu g\,m^{-3}$) | 90.8 | 89.1 | 56.9 | 53.8 | 18.9 |
| Area-weighted GOCI-derived $PM_{2.5}$ ($\mu g\,m^{-3}$) | 86.5 | 89.1 | 51.0 | 44.3 | 23.6 |
| $SO_4^{2-}$ ($\mu g\,m^{-3}$) | 12.8 | 14.0 | 9.2 | 13.1 | 5.1 |
| $NO_3^-$ ($\mu g\,m^{-3}$) | 14.5 | 16.1 | 8.5 | 4.2 | 2.1 |
| $NH_4^+$ ($\mu g\,m^{-3}$) | 8.9 | 9.8 | 5.7 | 3.3 | 2.2 |
| OC ($\mu g\,m^{-3}$) | 10.3 | 9.6 | 4.3 | 2.9 | 1.6 |
| BC ($\mu g\,m^{-3}$) | 6.3 | 5.2 | 2.6 | 1.6 | 0.8 |
| Dust ($\mu g\,m^{-3}$) | 9.1 | 8.3 | 4.9 | 4.4 | 2.9 |
| Sea Salt ($\mu g\,m^{-3}$) | 0.2 | 0.4 | 0.9 | 1.9 | 2.2 |
| OM ($\mu g\,m^{-3}$) | 17.1 | 15.7 | 7.4 | 5.4 | 3.0 |
| Population (million people) exposed to $PM_{2.5}$ exceeding IT-1 level | 37.8 | 88.8 | 98.3 | 432.8 | 1.5 |

variation in the north than south. The mixing height over northeastern China has strong seasonal variation with summer having an average mixing height from GEOS-5 that is 1.9 times higher than in winter. The GEOS-Chem simulation reveals that the increase of OM in winter is primarily driven by biofuel emissions from burning wood, animal waste and agricultural waste (Bond et al., 2004) for heating in eastern China. The spatial distribution of biofuel emission is primarily north of the Yangze River, especially from the North China Plain. The significant contribution from biofuel emissions to the OM concentration in our work is consistent with Bond et al. (2004) who found residential biofuel emissions were responsible for $\sim 70$ % of OC emissions in China. The increase of $NO_3^-$ in winter in Fig. 6 is consistent with prior attribution of the increase of $NO_3^-$ in winter to the favorable formation of $NH_4NO_3$ at low temperatures (Wang et al., 2013). Figure S1 in the Supplement shows the spatial distribution of $PM_{2.5}$ chemical components.

Table 1 shows the annual chemical composition of GOCI-derived $PM_{2.5}$ in regions outlined in Fig. 3 and in overall eastern China. SIA and OM are the most abundant species. Among the SIA components, $SO_4^{2-}$ and $NO_3^-$ concentrations are similar in the Beijing, Shandong and Shanghai regions, whereas in eastern China and northern Taiwan $SO_4^{2-}$ is the dominant component. OM concentrations in the Beijing and Shandong regions are considerably higher than in the other regions, similar to or even exceeding the concentrations of $SO_4^{2-}$ and $NO_3^-$. Our estimation of $PM_{2.5}$ composition is generally consistent with in situ measurements in prior studies. In Beijing, the concentrations of SIA in this work are similar to Zhang et al. (2013) who measured concentrations for 2009–2010 of $13.6 \pm 12.4\,\mu g\,m^{-3}$ for $SO_4^{2-}$, $11.3 \pm 10.8\,\mu g\,m^{-3}$ for $NO_3^-$ and $6.9 \pm 7.1\,\mu g\,m^{-3}$ for $NH_4^+$. Our SIA concentrations in Beijing are also comparable with Yang et al. (2011) who measured concentrations for 2005–2006 of $15.8 \pm 10.3\,\mu g\,m^{-3}$ for $SO_4^{2-}$, $10.1 \pm 6.09\,\mu g\,m^{-3}$ for $NO_3^-$ and $7.3 \pm 4.2\,\mu g\,m^{-3}$ for $NH_4^+$. The OC concentration in Beijing in this work is smaller than Zhang et al. (2013) of $16.9 \pm 10.0\,\mu g\,m^{-3}$ and Yang et al. (2011) of $24.5 \pm 12.0\,\mu g\,m^{-3}$. In Shandong and surrounding regions, our concentrations are smaller than in Cheng et al. (2011) by a factor of about 2, perhaps related to unresolved sources. Our results in Shanghai cluster are comparable with Yang et al. (2011) for 1999–2000, except the OC concentration ($4.3\,\mu g\,m^{-3}$) in this work is considerably lower than that of $16.8\,\mu g\,m^{-3}$ in Yang et al. (2011). In northern Taiwan, our $NO_3^-$ is similar to Fang et al. (2002) for 2001–2003, yet our estimations of $SO_4^{2-}$ and $NH_4^+$ are higher than Fang et al. (2002) by a factor of two, which could be driven by changes in emissions over the last decade. In summary, the chemical composition broadly represents in situ measurements with some location-dependent discrepancies.

### 3.4 Population exposure to ambient $PM_{2.5}$ in eastern China

We estimate the population exposure to ambient $PM_{2.5}$ in eastern China for 2013 at a spatial resolution of 6 km by 6 km using our GOCI-derived $PM_{2.5}$ and the Gridded Population of the World (GPW; Tobler et al., 1997) data for 2010 from the Socioeconomic Data and Applications Center (GPW version 3; http://sedac.ciesin.columbia.edu/). Table 1 also provides the population-weighted GOCI-derived $PM_{2.5}$ for re-

gions outlined in Fig. 3 and for overall eastern China. The population-weighted $PM_{2.5}$ exceeds the area-weighted for all regions except northern Taiwan and Shandong and surrounding regions. The overall population-weighted $PM_{2.5}$ concentration for eastern China for 2013 is 53.8 $\mu g\,m^{-3}$. The level of $PM_{2.5}$ for Beijing and Shandong regions in this study is similar to Ma et al. (2014) who suggested that the $PM_{2.5}$ concentration over the North China Plain for 2013 is 85–95 $\mu g\,m^{-3}$. The $PM_{2.5}$ concentration in eastern China in this study is also comparable with previous works. Van Donkelaar et al. (2015) estimated that the $PM_{2.5}$ concentration over eastern Asia for 2001–2010 is $50.3 \pm 24.3\,\mu g\,m^{-3}$. Geng et al. (2015) estimated that the $PM_{2.5}$ concentration in China for 2006–2012 is 71 $\mu g\,m^{-3}$, higher than our work. According to the World Health Organization (WHO) Air Quality Interim Target-1, an annual mean $PM_{2.5}$ concentration of 35 $\mu g\,m^{-3}$ or higher is associated with about 15 % increased risk of premature mortality. As shown in Table 1, population-weighted $PM_{2.5}$ for eastern China considerably exceeds the Interim Target-1 level of $PM_{2.5}$ concentration, especially in Beijing and Shandong regions where the $PM_{2.5}$ concentration is almost triple the Interim Target-1 level. These elevated concentrations threaten the health of 433 million inhabitants (Table 1) in eastern China who live in regions that exceed this target.

## 4 Conclusions

We estimated the ground-level concentration of $PM_{2.5}$ in eastern China for 2013 using AOD retrieved from the GOCI satellite instrument, coupled with the relationship of AOD to $PM_{2.5}$ simulated by a global chemical transport model (GEOS-Chem). GOCI-derived $PM_{2.5}$ was compared with in situ measurements throughout eastern China.

We applied a set of filters to GOCI AOD to remove cloud contamination. The filtered GOCI AOD showed significant agreement with AERONET AOD at Beijing and northern Taiwan (MFB of 6.7 to −1.2 %). We also evaluated the simulated relationship of $PM_{2.5}$ and AOD from GEOS-Chem by using an empirical relationship calculated from nearly collocated ground-based $PM_{2.5}$ monitors and AERONET AOD stations. A high degree of consistency was observed between the GEOS-Chem simulation and ground-based measurements with MFB of −0.52 to 8.0 %.

The GOCI-derived $PM_{2.5}$ were highly consistent with in situ measurements, capturing the similar seasonal and spatial distribution throughout eastern China. The highest $PM_{2.5}$ concentrations were found in winter over northern regions. The annual averages of GOCI-derived $PM_{2.5}$ were strongly correlated ($r^2 = 0.66$) with surface measurements with a slope near unity (1.01). Monthly comparison of GOCI-derived $PM_{2.5}$ with ground-based measurements across the entire region of eastern China was also in good agreement with rRMSE = 18.9 %. The exclusion of our cloud-screening filters in GOCI retrievals would introduce significant bias in GOCI-derived $PM_{2.5}$, especially in summer and would increase the rRMSE by a factor of 1.7–5.3.

The chemical composition of GOCI-derived $PM_{2.5}$ revealed that secondary inorganic aerosols (SIA; $SO_4^{2-}$, $NO_3^-$, $NH_4^+$) and organic matter (OM) dominated throughout the year. $NO_3^-$ had a winter maximum due to aerosol thermodynamics. OM increased by a factor of 2 in winter, which was primarily driven by biofuel emission for heating in northern China. Dust played an important role in spring and fall.

The population-weighted GOCI-derived $PM_{2.5}$ for 2013 at 6 km by 6 km resolution in eastern China was 53.8 $\mu g\,m^{-3}$, suggesting ∼ 400 million people in China live in regions with $PM_{2.5}$ concentrations exceeding the suggested 35 $\mu g\,m^{-3}$ by the World Health Organization (WHO) Air Quality Interim Target-1, of which ∼ 130 million people in Beijing and Shandong regions are seriously threatened by even higher $PM_{2.5}$ concentrations. Population-weighted $PM_{2.5}$ of pixels containing ground-based monitors is much higher at 82.4 $\mu g\,m^{-3}$, suggesting the value of the newly established $PM_{2.5}$ network to monitor these seriously polluted regions.

The satellite measurements of AOD from the GOCI instrument coupled with the relationship between AOD and $PM_{2.5}$ simulated by a chemical transport model have the potential to provide a unique synopsis of ground-level $PM_{2.5}$ concentrations at fine spatial resolution in the most polluted and populated part of China. Further development of this capability will depend on both the quality of GOCI aerosol products and the aerosol simulation. Assimilating satellite observations of trace gases from the forthcoming GEMS (Geostationary Environment Spectrometer) geostationary platform would provide additional constraints on $PM_{2.5}$ composition.

**The Supplement related to this article is available online at doi:10.5194/acp-15-13133-2015-supplement.**

*Acknowledgements.* We are grateful to the GOCI, AERONET, CEMC, TEPA and SPARTAN for providing available data used in this study. Funding for this work was provided by NSERC (Natural Sciences and Engineering Research Council of Canada) and by an Izaak Walton Killiam Memorial Scholarship for J.-W. Xu. Computational facilities are partially provided by ACEnet, the regional high performance computing consortium for universities in Atlantic Canada.

Edited by: M. Tesche

## References


Bey, I., Jacob, D. J., Yantosca, R. M., Logan, J. A., Field, B. D., Fiore, A. M., Li, Q. B., Liu, H .G. Y., Mickley, L. J., and Schultz, M. G.: Global modeling of tropospheric chemistry with assimilated meteorology: Model description and evaluation, J. Geophys. Res., 106, 23073–23095, doi:10.1029/2001JD000807, 2001.

Bond, T. C., Streets, D. G., Yarber, K. F., Nelson, S. M., Woo, J.-H., and Klimont, Z.: A technology-based global inventory of black and organic carbon emissions from combustion, J. Geophys. Res., 109, D14203, doi:10.1029/2003JD003697, 2004.

Boys, B. L., Martin, R. V., van Donkelaar, A., MacDonell, R. J., Hsu, N. C., Cooper, M. J., Yantosca, R. M., Lu, Z., Streets, D. G., Zhang, Q., and Wang, S. W.: Fifteen-Year Global Time Series of Satellite-Derived Fine Particulate Matter, Environ. Sci. Technol., 48, 11109–11118, 2014.

Cheng, S., Yang, L. X., Zhou, X., Wang, Z., Zhou, Y., Gao, X., Nie, W., Wang, X., Xu, P., and Wang, W.: Evaluating $PM_{2.5}$ ionic components and source apportionment in Jinan, China from 2004 to 2008 using trajectory statistical methods, J. Environ. Monit., 13, 1662–1671, 2011.

Cho, Y. and Youn, H.: Characteristics of COMS Meteorological Imager, in: Sensors, Systems, and Next-Generation Satellites X, Proc. SPIE, Stockholm, Sweden, doi:10.1117/12.688393, 3 October 2006.

CNAAQS, GB3095-2012, Ministry of Environmental Protection of the People's Republic of China: Chinese National Ambient Air Quality Standard, Beijing, China, 2012.

Fairlie, T. D., Jacob, D. J., and Park, R. J.: The impact of transpacific transport of mineral dust in the United States, Atmos. Environ., 41, 1251–1266, doi:10.1016/j.atmosenv.2006.09.048, 2007.

Fang, G., Chang, C., Wu, Y., Fu, P. P., Yang, C., Chen, C., and Chang, S.: Ambient suspended particulate matters and related chemical species study in central Taiwan, Taichung during 1998–2001, Atmos. Environ., 36, 1921–1928, 2002.

Fischer, J. A., Jacob, D. J., Wang, Q., Bahreini, R., Carouge, C. C., Cubison, M. J., Dibb, J. E., Diehl, T., Jimenez, J. L., and Leibensperger, E. M.: Sources, distribution, and acidity of sulfate–ammonium aerosol in the Arctic in winter–spring, Atmos. Environ., 45, 7301–7318, 2011.

Fountoukis, C. and Nenes, A.: ISORROPIA II: a computationally efficient thermodynamic equilibrium model for $K^+$-$Ca^{2+}$-$Mg^{2+}$-$NH_4^+$-$Na^+$-$SO_4^{2-}$-$NO_3^-$-$Cl^-$-$H_2O$ aerosols, Atmos. Chem. Phys., 7, 4639–4659, doi:10.5194/acp-7-4639-2007, 2007.

Fu, T., Jacob, D. J., Wittrock, F., Burrows, J. P., Vrekoussis, M., and Henze, D. K.: Global budgets of atmospheric glyoxal and methylglyoxal, and implications for formation of secondary organic aerosols, J. Geophys. Res., 113, D15303, doi:10.1029/2007JD009505, 2008.

Geng, G., Zhang, Q., Martin, R. V., van Donkelaar, A., Huo, H., Che, H., Lin, J., and He, K.: Estimating long-term $PM_{2.5}$ concentrations in China using satellite-based aerosol optical depth and a chemical transport model, Remote Sens. Environ., 166, 262–270, doi:10.1016/j.rse.2015.05.016, 2015.

Goldberg, M.: A systematic review of the relation between long-term exposure to ambient air pollution and chronic diseases, Rev. Environ. Health, 23, 243–298, doi:10.1515/REVEH.2008.23.4.243, 2008.

Guenther, A., Karl, T., Harley, P., Wiedinmyer, C., Palmer, P. I., and Geron, C.: Estimates of global terrestrial isoprene emissions using MEGAN (Model of Emissions of Gases and Aerosols from Nature), Atmos. Chem. Phys., 6, 3181–3210, doi:10.5194/acp-6-3181-2006, 2006.

He, K., Yang, F., Ma, Y., Zhang, Q., Yao, X., Chan, C. K., Cadle, S., Chan, T., and Mulawa, P.: The characteristics of $PM_{2.5}$ in Beijing, China, Atmos. Environ., 35, 4959, doi:10.1016/S1352-2310(01)00301-6, 2001.

Heald, C. L., Collett Jr., J. L., Lee, T., Benedict, K. B., Schwandner, F. M., Li, Y., Clarisse, L., Hurtmans, D. R., Van Damme, M., Clerbaux, C., Coheur, P.-F., Philip, S., Martin, R. V., and Pye, H. O. T.: Atmospheric ammonia and particulate inorganic nitrogen over the United States, Atmos. Chem. Phys., 12, 10295–10312, doi:10.5194/acp-12-10295-2012, 2012.

Henze, D. K. and Seinfeld, J. H.: Global secondary organic aerosol from isoprene oxidation, Geophys. Res. Lett., 33, L09812, doi:10.1029/2006GL025976, 2006.

Henze, D. K., Seinfeld, J. H., Ng, N. L., Kroll, J. H., Fu, T.-M., Jacob, D. J., and Heald, C. L.: Global modeling of secondary organic aerosol formation from aromatic hydrocarbons: high- vs. low-yield pathways, Atmos. Chem. Phys., 8, 2405–2420, doi:10.5194/acp-8-2405-2008, 2008.

Holben, B., Eck, T., Slutsker, I., Tanre, D., Buis, J., Setzer, A., Vermote, E., Reagan, J., Kaufman, Y., and Nakajima, T.: AERONET – A federated instrument network and data archive for aerosol characterization, Remote Sens. Environ., 66, 1–16, 1998.

Holben, B., Tanre, D., Smirnov, A., Eck, T., Slutsker, I., Abuhassan, N., Newcomb, W., Schafer, J., Chatenet, B., and Lavenu, F.: An emerging ground-based aerosol climatology: Aerosol optical depth from AERONET, J. Geophys. Res. (1984–2012), 106, 12067–12097, 2001.

Hu, X., Waller, L. A., Al-Hamdan, M. Z., Crosson, W. L., Estes Jr., M. G., Estes, S. M., Quattrochi, D. A., Sarnat, J. A., and Liu, Y.: Estimating ground-level $PM_{2.5}$ concentrations in the southeastern US using geographically weighted regression, Environ. Res., 121, 1–10, 2013.

Hyer, E. J., Reid, J. S., and Zhang, J.: An over-land aerosol optical depth data set for data assimilation by filtering, correction, and aggregation of MODIS Collection 5 optical depth retrievals, Atmos. Meas. Tech., 4, 379–408, doi:10.5194/amt-4-379-2011, 2011.

Jaeglé, L., Quinn, P. K., Bates, T. S., Alexander, B., and Lin, J.-T.: Global distribution of sea salt aerosols: new constraints from in situ and remote sensing observations, Atmos. Chem. Phys., 11, 3137–3157, doi:10.5194/acp-11-3137-2011, 2011.

Jiang, X., Zhang, Q., Zhao, H., Geng, G., Peng, L., Guan, D., Kan, H., Huo, H., Lin, J., Brauer, M., Martin, R. V., and He, K.: Revealing the hidden health costs embodied in Chinese exports, Environ. Sci. Technol., 49, 4381–4388, 10.1021/es506121s, 2015.

Kang, G., Youn, H. S., Choi, S. B., and Coste P., Radiometric calibration of COMS geostationary ocean color imager, IEEE T. Geosci. Remote, 6361, 636112, doi:10.1117/12.689888, 2006.

Kloog, I., Nordio, F., Coull, B. A., and Schwartz, J.: Incorporating local land use regression and satellite aerosol optical depth in a hybrid model of spatiotemporal $PM_{2.5}$ exposures in the Mid-Atlantic states, Environ. Sci. Tech., 46, 11913–11921, 2012.

Laden, F., Schwartz, J., Speizer, F. E., and Dockery, D. W.: Reduction in fine particulate air pollution and mortality: extended follow-up of the Harvard Six Cities study, Am. J. Resp. Crit. Care, 173, 667–672, 2006.

Lee, J., Kim, J., Song, C. H., Ryu, J., Ahn, Y., and Song, C. K.: Algorithm for retrieval of aerosol optical properties over the ocean from the Geostationary Ocean Color Imager, Remote Sens. Environ., 114, 1077, doi:10.1016/j.rse.2009.12.021, 2010.

Lee, J., Kim, J., Yang, P., and Hsu, N. C.: Improvement of aerosol optical depth retrieval from MODIS spectral reflectance over the global ocean using new aerosol models archived from AERONET inversion data and tri-axial ellipsoidal dust database, Atmos. Chem. Phys., 12, 7087–7102, doi:10.5194/acp-12-7087-2012, 2012.

Liao, H., Henze, D. K., Seinfeld, J. H., Wu, S., and Mickley, L. J.: Biogenic secondary organic aerosol over the United States: Comparison of climatological simulations with observations, J. Geophys. Res., 112, D06201, doi:10.1029/2006JD007813, 2007.

Lim, S. S., Vos, T., Flaxman, A. D., Danaei, G., Shibuya, K., Adair-Rohani, H., Al Mazroa, M. A., Amann, M., Anderson, H. R., Andrews, K. G., Aryee, M., Atkinson, C., Bacchus, L. J., Bahalim, A. N., Balakrishnan, K., Balmes, J., Barker-Collo, S., Baxter, A., Bell, M. L., Blore, J. D., Blyth, F., Bonner, C., Borges, G., Bourne, R., Boussinesq, M., Brauer, M., Brooks, P., Bruce, N. G., Brunekreef, B., Bryan-Hancock, C., Bucello, C., Buchbinder, R., Bull, F., Burnett, R. T., Byers, T. E., Calabria, B., Carapetis, J., Carnahan, E., Chafe, Z., Charlson, F., Chen, H., Chen, J. S., Cheng, A. T., Child, J. C., Cohen, A., Colson, K. E., Cowie, B. C., Darby, S., Darling, S., Davis, A., Degenhardt, L., Dentener, F., Des Jarlais, D. C., Devries, K., Dherani, M., Ding, E. L., Dorsey, E. R., Driscoll, T., Edmond, K., Ali, S. E., Engell, R. E., Erwin, P. J., Fahimi, S., Falder, G., Farzadfar, F., Ferrari, A., Finucane, M. M., Flaxman, S., Fowkes, F. G. R., Freedman, G., Freeman, M. K., Gakidou, E., Ghosh, S., Giovannucci, E., Gmel, G., Graham, K., Grainger, R., Grant, B., Gunnell, D., Gutierrez, H. R., Hall, W., Hoek, H. W., Hogan, A., Hosgood III, H. D., Hoy, D., Hu, H., Hubbell, B. J., Hutchings, S. J., Ibeanusi, S. E., Jacklyn, G. L., Jasrasaria, R., Jonas, J. B., Kan, H., Kanis, J. A., Kassebaum, N., Kawakami, N., Khang, Y., Khatibzadeh, S., Khoo, J., Kok, C., Laden, F., Lalloo, R., Lan, Q., Lathlean, T., Leasher, J. L., Leigh, J., Li, Y., Lin, J. K., Lipshultz, S. E., London, S., Lozano, R., Lu, Y., Mak, J., Malekzadeh, R., Mallinger, L., Marcenes, W., March, L., Marks, R., Martin, R., McGale, P., McGrath, J., Mehta, S., Memish, Z. A., Mensah, G. A., Merriman, T. R., Micha, R., Michaud, C., Mishra, V., Hanafiah, K. M., Mokdad, A. A., Morawska, L., Mozaffarian, D., Murphy, T., Naghavi, M., Neal, B., Nelson, P. K., Nolla, J. M., Norman, R., Olives, C., Omer, S. B., Orchard, J., Osborne, R., Ostro, B., Page, A., Pandey, K. D., Parry, C. D., Passmore, E., Patra, J., Pearce, N., Pelizzari, P. M., Petzold, M., Phillips, M. R., Pope, D., Pope III, C. A., Powles, J., Rao, M., Razavi, H., Rehfuess, E. A., Rehm, J. T., Ritz, B., Rivara, F. P., Roberts, T., Robinson, C., Rodriguez-Portales, J. A., Romieu, I., Room, R., Rosenfeld, L. C., Roy, A., Rushton, L., Salomon, J. A., Sampson, U., Sanchez-Riera, L., Sanman, E., Sapkota, A., Seedat, S., Shi, P., Shield, K., Shivakoti, R., Singh, G. M., Sleet, D. A., Smith, E., Smith, K. R., Stapelberg, N. J., Steenland, K., Stöckl, H., Stovner, L. J., Straif, K., Straney, L., Thurston, G. D., Tran, J. H., Van Dingenen, R., van Donkelaar, A., Veerman, J. L., Vijayakumar, L., Weintraub, R., Weissman, M. M., White, R. A., Whiteford, H., Wiersma, S. T., Wilkinson, J. D., Williams, H. C., Williams, W., Wilson, N., Woolf, A. D., Yip, P., Zielinski, J. M., Lopez, A. D., Murray, C. J., and Ezzati, M.: A comparative risk assessment of burden of disease and injury attributable to 67 risk factors and risk factor clusters in 21 regions, 1990–2010: a systematic analysis for the Global Burden of Disease Study 2010, The Lancet, 380, 2224–2260, doi:10.1016/S0140-6736(12)61766-8, 2012.

Liu, Y., Park, R. J., Jacob, D. J., Li, Q., Kilaru, V., and Sarnat, J. A.: Mapping annual mean ground-level $PM_{2.5}$ concentrations using Multiangle Imaging Spectroradiometer aerosol optical thickness over the contiguous United States, J. Geophys. Res. (1984–2012), 109, D22206, doi:10.1029/2004JD005025, 2004.

Liu, Y., Paciorek, C. J., and Koutrakis, P.: Estimating regional spatial and temporal variability of $PM_{2.5}$ concentrations using satellite data, meteorology, and land use information, Environ. Health Perspect., 117, 886–892, 2009.

Ma, Z., Hu, X., Huang, L., Bi, J., and Liu, Y.: Estimating ground-level $PM_{2.5}$ in China using satellite remote sensing, Environ. Sci. Tech., 48, 7436–7444, 2014.

Martin, R. V., Jacob, D. J., Yantosca, R. M., Chin, M., and Ginoux, P.: Global and regional decreases in tropospheric oxidants from photochemical effects of aerosols, J. Geophys. Res., 108, 4097, doi:10.1029/2002JD002622, 2003.

Mu, M., Randerson, J., Van der Werf, G., Giglio, L., Kasibhatla, P., Morton, D., Collatz, G., DeFries, R., Hyer, E., and Prins, E.: Daily and 3-hourly variability in global fire emissions and consequences for atmospheric model predictions of carbon monoxide, J. Geophys. Res. (1984–2012), 116, D24303, doi:10.1029/2011JD016245, 2011.

Murray, L. T., Jacob, D. J., Logan, J. A., Hudman, R. C., and Koshak, W. J.: Optimized regional and interannual variability of lightning in a global chemical transport model constrained by LIS/OTD satellite data, J. Geophys. Res. (1984–2012), 117, D20307, doi:10.1029/2012JD017934, 2012.

Ohara, T., Akimoto, H., Kurokawa, J., Horii, N., Yamaji, K., Yan, X., and Hayasaka, T.: An Asian emission inventory of anthropogenic emission sources for the period 1980–2020, Atmos. Chem. Phys., 7, 4419–4444, doi:10.5194/acp-7-4419-2007, 2007.

Olivier, J. G. J. and Berdowski, J. J. M.: Global emissions sources and sinks, in: The Climate System, edited by: Berdowski, J., Guicherit, R., and Heij, B. J., A. A. Balkema Publishers/Swets & Zeitlinger Publishers, Lisse, the Netherlands, 33–78, 2001.

Park, M. E., Song, C. H., Park, R. S., Lee, J., Kim, J., Lee, S., Woo, J.-H., Carmichael, G. R., Eck, T. F., Holben, B. N., Lee, S.-S., Song, C. K., and Hong, Y. D.: New approach to monitor transboundary particulate pollution over Northeast Asia, Atmos. Chem. Phys., 14, 659–674, doi:10.5194/acp-14-659-2014, 2014.

Park, R. J., Jacob, D. J., Chin M., and Martin, R. V.: Sources of carbonaceous aerosols over the United States and implications for natural visibility, J. Geophys. Res, 108, 4355, doi:10.1029/2002JD003190, 2003.

Park, R. J., Jacob, D. J., Field, B. D., Yantosca, R. M., and Chin, M.: Natural and transboundary pollution influences on sulfate-nitrate-ammonium aerosols in the United States: implications for policy, J. Geophys. Res., 109, D15204, doi:10.1029/2003JD004473, 2004.

Philip, S., Martin, R. V., Pierce, J. R., Jimenez, J. L., Zhang, Q., Canagaratna, M. R., Spracklen, D. V., Nowlan, C. R., Lamsal, L. N., Cooper, M. J., and Krotkov, N. A.: Spatially and seasonally resolved estimate of the ratio of global organic matter to organic carbon, Atmos. Environ., 87, 34–40, doi:10.1016/j.atmosenv.2013.11.065, 2014.

Pye, H. O. T., Liao, H., Wu, S., Mickley, L. J., Jacob, D. J., Henze, D. K., and Seinfeld, J. H.: Effect of changes in climate and emissions on future sulfate-nitrate-ammonium aerosol levels in the United States, J. Geophys. Res., 114, D01205, doi:10.1029/2008JD010701, 2009.

Ridley, D. A., Heald, C. L., and Ford, B.: North African dust export and deposition: A satellite and model perspective., J. Geophys. Res., 117, D02202, doi:10.1029/2011JD016794, 2012.

Silva, R. A., West, J. J., Zhang, Y., Anenberg, S. C., Lamarque, J., Shindell, D. T., Collins, W. J., Dalsoren, S., Faluvegi, G., and Folberth, G.: Global premature mortality due to anthropogenic outdoor air pollution and the contribution of past climate change, Environ. Res. Lett., 8, 034005, doi:10.1088/1748-9326/8/3/034005, 2013.

Smirnov, A., Holben, B., Eck, T., Dubovik, O., and Slutsker, I.: Cloud-screening and quality control algorithms for the AERONET database, Remote Sens. Environ., 73, 337–349, 2000.

Snider, G., Weagle, C. L., Martin, R. V., van Donkelaar, A., Conrad, K., Cunningham, D., Gordon, C., Zwicker, M., Akoshile, C., Artaxo, P., Anh, N. X., Brook, J., Dong, J., Garland, R. M., Greenwald, R., Griffith, D., He, K., Holben, B. N., Kahn, R., Koren, I., Lagrosas, N., Lestari, P., Ma, Z., Vanderlei Martins, J., Quel, E. J., Rudich, Y., Salam, A., Tripathi, S. N., Yu, C., Zhang, Q., Zhang, Y., Brauer, M., Cohen, A., Gibson, M. D., and Liu, Y.: SPARTAN: a global network to evaluate and enhance satellite-based estimates of ground-level particulate matter for global health applications, Atmos. Meas. Tech., 8, 505–521, doi:10.5194/amt-8-505-2015, 2015.

Stettler, M. E. J., Eastham, S., and Barrett, S. R. H.: Air quality and public health impacts of UK airports. Part I: Emissions, Atmos. Environ., 45, 5415–5424, 2011.

Tao, J., Shen, Z., Zhu, C., Yue, J., Cao, J., Liu, S., Zhu, L., and Zhang, R.: Seasonal variations and chemical characteristics of sub-micrometer particles (PM1) in Guangzhou, China, Atmos. Res., 115, 222–231, doi:10.1016/j.atmosres.2012.06.025, 2012.

Tobler, W., Deichmann, U., Gottsegen, J., and Maloy, K.: World population in a grid of spherical quadrilaterals, Int. J. Popul. Geogr., 3, 203–225, 1997.

van Donkelaar, A., Martin, R. V., and Park, R. J.: Estimating ground-level $PM_{2.5}$ using aerosol optical depth determined from satellite remote sensing, J. Geophys. Res (1984–2012), 111, D21201, doi:10.1029/2005JD006996, 2006.

van Donkelaar, A., Martin, R. V., Brauer, M., Kahn, R., Levy, R., Verduzco, C., and Villeneuve, P. J.: Global estimates of ambient fine particulate matter concentrations from satellite-based aerosol optical depth: development and application, Environ. Health Perspect., 118, 847–855, doi:10.1289/ehp.0901623, 2010.

van Donkelaar, A., Martin, R. V., Brauer, M., and Boys, B. L.: Use of Satellite Observations for Long-Term Exposure Assessment of Global Concentrations of Fine Particulate Matter, Environ. Health Perspect., 123, 135–143, doi:10.1289/ehp.1408646, 2015.

Walker, J. M., Philip, S., Martin, R. V., and Seinfeld, J. H.: Simulation of nitrate, sulfate, and ammonium aerosols over the United States, Atmos. Chem. Phys., 12, 11213–11227, doi:10.5194/acp-12-11213-2012, 2012.

Wang, J. and Christopher, S. A.: Intercomparison between satellite-derived aerosol optical thickness and $PM_{2.5}$ mass: Implications for air quality studies, Geophys. Res. Lett., 30, 2095, doi:10.1029/2003GL018174, 2003.

Wang, Y., Logan, J. A., and Jacob D. J.: Global simulation of tropospheric $O_3$-$NO_x$-hydrocarbon chemistry: 2. Model evaluation and global ozone budget, J. Geophys. Res. (1984–2012), 103, 10757–10767, 1998.

Wang, Y., McElroy, M. B., Jacob, D. J., and Yantosca, R. M.: A nested grid formulation for chemical transport over Asia: Applications to CO, J. Geophys. Res., 109, D22307, doi:10.1029/2004JD005237, 2004.

Wang, Y., Zhang, Q. Q., He, K., Zhang, Q., and Chai, L.: Sulfate-nitrate-ammonium aerosols over China: response to 2000–2015 emission changes of sulfur dioxide, nitrogen oxides, and ammonia, Atmos. Chem. Phys., 13, 2635–2652, doi:10.5194/acp-13-2635-2013, 2013.

Yang, F., Tan, J., Zhao, Q., Du, Z., He, K., Ma, Y., Duan, F., Chen, G., and Zhao, Q.: Characteristics of $PM_{2.5}$ speciation in representative megacities and across China, Atmos. Chem. Phys., 11, 5207–5219, doi:10.5194/acp-11-5207-2011, 2011.

Ye, B., Ji, X., Yang, H., Yao, X., Chan, C. K., Cadle, S. H., Chan, T., and Mulawa, P. A.: Concentration and chemical composition of $PM_{2.5}$ in Shanghai for a 1-year period, Atmos. Environ., 37, 499–510, doi:10.1016/S1352-2310(02)00918-4, 2003.

Yienger, J. and Levy, H.: Empirical model of global soil biogenic $NO_x$ emissions, J. Geophys. Res. (1984–2012), 100, 11447–11464, 1995.

Zhang, Q., Streets, D. G., Carmichael, G. R., He, K. B., Huo, H., Kannari, A., Klimont, Z., Park, I. S., Reddy, S., Fu, J. S., Chen, D., Duan, L., Lei, Y., Wang, L. T., and Yao, Z. L.: Asian emissions in 2006 for the NASA INTEX-B mission, Atmos. Chem. Phys., 9, 5131–5153, doi:10.5194/acp-9-5131-2009, 2009.

Zhang, R., Jing, J., Tao, J., Hsu, S.-C., Wang, G., Cao, J., Lee, C. S. L., Zhu, L., Chen, Z., Zhao, Y., and Shen, Z.: Chemical characterization and source apportionment of $PM_{2.5}$ in Beijing: seasonal perspective, Atmos. Chem. Phys., 13, 7053–7074, doi:10.5194/acp-13-7053-2013, 2013.

Zhang, X. Y., Wang, Y. Q., Zhang, X. C., Guo, W., and Gong, S. L.: Carbonaceous aerosol composition over various regions of China during 2006, J. Geophys. Res., 113, D14111, doi:10.1029/2007JD009525, 2008.

Zhao, P. S., Dong, F., He, D., Zhao, X. J., Zhang, X. L., Zhang, W. Z., Yao, Q., and Liu, H. Y.: Characteristics of concentrations and chemical compositions for $PM_{2.5}$ in the region of Beijing, Tianjin, and Hebei, China, Atmos. Chem. Phys., 13, 4631–4644, doi:10.5194/acp-13-4631-2013, 2013.